arXiv:astro-ph/9812392v1 21 Dec 1998

Resonant Absorption in the AGN spectra emerging from photoionized gas: differences between steep and flat ionizing continua

Fabrizio Nicastro[1,2,3], Fabrizio Fiore[1,2,4], and Giorgio Matt[5]

[1] Harvard-Smithsonian Center for Astrophysics

60 Garden st. Cambridge Ma. 02138 USA

[2] Osservatorio Astronomico di Roma

via Osservatorio, Monteporzio-Catone (RM), I00040 Italy

[3] Istituto di Astrofisica Spaziale - CNR

Via del Fosso del Cavaliere, Roma, I-00133 Italy

[4] BeppoSAX Science Data Center

via Corcolle 19, Roma I00100 Italy

[5] Dipartimento di Fisica, Università degli Studi "Roma Tre"

Via della Vasca Navale 84, Roma, I00146 Italy

version: 18 November 1998

Received _____; accepted _____

ABSTRACT

We present photoionization models accounting for both photoelectric and resonant absorption. Resonance absorption lines from C, O, Ne, Mg, Si S and Fe between 0.1 and 10 keV are treated. In particular we consider the complex of almost 60 strong Fe L absorption lines around 1 keV. We calculate profiles, intensities and equivalent widths of each line, considering both Doppler and natural broadening mechanisms. Doppler broadening includes a term accounting for turbulence of the gas along the line of sight.

We computed spectra transmitted by gas illuminated by drastically different ionizing continua and compared them to spectra observed in flat X-ray spectrum, broad optical emission line type 1 AGN, and steep X-ray spectrum, narrow optical emission line type 1 AGN. We show that the $\sim$ 1 keV absorption feature observed in moderate resolution X-ray spectra of several Narrow Line Seyfert 1 galaxies can be explained by photoionization models, taking into account for resonance absorption, without requiring relativistic outflowing velocities of the gas, if the physical properties of these absorbers are close to those found in flat X-ray spectrum Seyfert 1 galaxies.

We finally present simulations of the spectra emerging from gas illuminated by both steep and flat ionizing continua, as seen by the AXAF High energy Transmission Gratings and the baseline Constellation-X calorimeter. We discuss briefly the relevant physics which can be investigated with these instruments.

1. Introduction

The ROSAT (Trümper 1983) PSPC (Pfefferman et al. 1987) has found a large spread in the spectral indices of type 1 AGN: $0.5 < \alpha_E < 3$ ($f(E) = E^{-\alpha_E}$; Laor et al 1997, Walter & Fink, 1993, Fiore et al. 1994). This remarkably broad soft X-ray spectral index distribution appears not to be at random, but rather it is strongly correlated with other important optical and X-ray properties of these objects. Objects with narrower Hβ (1000 < FWHM< 2000 km s^{-1}) and smaller [OIII]/Hβ (< 1) ratio are systematically steeper in soft X-rays ($\alpha_E > 1.5$) than AGN with broad (FWHM> 2000 km s^{-1}) permitted lines and greater [OIII]/H β ratio (1 <[OIII]/Hβ < 3, $\alpha_{PSPC} < 1.5$). In particular most of the so called Narrow Line Seyfert 1 Galaxies (NLSy1) show a steep 0.2-2 keV continuum (Boller et al 1996). In the 2–10 keV energy range narrow optical emission line quasars have still a somewhat steeper spectrum compared to broad optical emission line quasars. The spread of the 2-10 keV spectral index is however smaller than that of the 0.1-2 keV, PSPC one (Brandt et al., 1997). It has been suggested that these properties are correlated with the accretion rate (Pounds et al 1995, Laor et al 1997, Fiore et al 1998a,b).

Ionized gas, modifying the AGN X-ray spectrum, has been detected in about half of the bright, X-ray flat, broad optical emission line type 1 AGN studied by ASCA (Reynolds, 1997, George, 1998). The main features imprinted by the ionized gas on the X-ray spectrum are the OVII and OVIII K absorption edges at 0.74 and 0.87 keV. **As already pointed out by George et al. (1998), the similarity of the parameters of these features among different sources in the both the Reynolds (1997) and the George et al. (1998) samples implies that 'warm' absorbers in AGN have all roughly similar ionization structure, despite of the broad range of ionizing luminosity (i.e. about 3 orders of magnitude, from $\sim 10^{41}$ to 10^{44} erg s^{-1}).** In terms of the ionization parameter U, the presence in the gas of He-like and H-like ions of C, O and Ne as dominant ionic species, implies a narrow range of LogU=0.5-1.5 (Nicastro et al, 1998a). This is consistent with the location of the 'warm' gas at radii scaling with the root square of the luminosity. The column densities of the Reynolds sample are distributed in the range logN_H=21-23, but the standard deviation of the distribution is rather small, $\sigma_{\log N_H} = 0.3$, again indicating a relative uniformity in the physical properties of this AGN component. Several type 1 AGN showing ionized absorption features in X-ray also show high ionization UV absorption lines (namely OVI, NV, CIV, CIII]), over-imposed to the broad emission lines and systematically blue-shifted with respect to them (Mathur et al., 1994, 1995, 1998). **The widths of these absorption lines are tipically much broader than the associated thermal broadening, suggesting turbulence velocities of the absorber.** The UV and the X-ray absorbers have ionization states compatible with each other, which

supports the identification of these two components (Mathur et al., 1994, 1995, 1997, 1998). **In one of these cases (the Seyfert 1 galaxy NGC 3516) the total column density implied by some strong UV absorption lines is larger than that required by the X-ray absorption features (Kriss et al., 1996a,b). However it is well possible that more than one kinematic components contribute to the total intensity and equivalent width of the UV lines and that only one of those is physically associated with the X-ray absorber (Mathur et al., 1997).** The UV absorption lines may be produced in a turbulent outflowing wind intercepting the line of sight (possibly driven out by radiative acceleration). The outflowing velocities of the UV 'warm' gas span the range $v_{out} \sim 100 - 2000$ km s^{-1} (Mathur et al. 1994, 1995, 1997), and a similar range has been estimated for the dispersion velocities σ_v along the line of sight.

On the other hand, deep absorption features at the energies of the K edges of high ionized oxygen have never been observed in the 0.1-2 keV spectra of soft X-ray steep spectrum, narrow optical emission line type 1 AGN. Detections of deep oxygen edges have been reported for two sources previously classified as NLSy1 (IRAS 17020+4544, Leighly et al., 1997; Mrk 766, Matt et al., 1998, RE J2248-511, Puchnarewicz et al., 1995). During the ASCA (0.5-10 keV) and BeppoSAX (0.1-10 keV) observations the two sources have a rather flat X-ray continuum ($\alpha_E \sim 1$) and therefore cannot be considered X-ray steep AGNs. Large variations of the X-ray spectral shape have already been observed in the past (e.g. 1H 0419-577, NGC 4051, RE J2248-511, Guainazzi et al 1998a,b, Turner et al 1998, Puchnarewicz et al., 1995). **It is well possible that a population of (perhaps low mass) AGN does exist, switching between soft, high states and hard, low states (depending possibly on the accretion rate), and therefore classified in a way or in the other depending on the observed state (in analogy to what seen in Galactic Black Hole Candidates).**

Despite the lack of oxygen edges, steep soft X-ray spectrum, narrow optical emission line, type 1 AGN are usually far from being featureless (Brandt, 1995; Hayashida, 1997). ASCA has found large residuals between 1 and 2 keV, after subtracting the appropriate continuum, in at least 4 cases (Leighly et al., 1997, Fiore et al., 1998a). The interpretation of these features is not unique, given the relatively modest spectral resolution of the ASCA SIS and the complexity of the continua. Leighly et al. (1997) interprets the features found in the three NLSy1 studied in terms of OVII and OVIII resonance absorption lines blushifted by ~ 0.5 c. Fiore et al. (1998a) interpret the feature found in PG1244+026 in terms of either an emission line at 0.92 keV or Fe XVIII and Fe XVII resonant absorption blueshifted by ~ 0.3 c.

Photoionization models used to fit and interpret AGN spectra usually deal with photoelectric absorption only. Matt (1994) and Krolik & Kriss (1995) were the first to point out the importance of X–ray resonant absorption lines in ionized absorbers. Here we calculate in detail photoionization models, including all the relevant resonant absorption lines, and study the dependence of the transmitted spectrum on the exact shape of the ionizing continuum. We find that the phenomenologies observed in both broad optical emission lines type 1 AGN and NLSy1 galaxies can be explained in terms of their quite different ionizing continua, provided that, for a given luminosity, the radial distance of the gas clouds from the ionizing source (in units of gravitational radii) and the gas density are similar in both classes of objetcs.

Netzer (1993, 1996) discussed the relevance of recombination and fluorescent emission lines, provided that the covering factor of the ionized matter is significant, while Krolik & Kriss (1995) and Matt, Brandt & Fabian (1996) pointed out that resonant scattering lines can be even more intense. Here, for the sake of simplicity, we do not consider any line emission, and therefore our model is strictly valid only if the covering factor is negligible (see next section).

In section 2 we present our photoelectric+resonant absorption model, and discuss the relevant physics. Section 3 compares the transmitted spectra computed with our models for two different ionizing continua with the spectra of a broad optical emission line type 1 AGN and a NLSy1 galaxy actually observed by ASCA ($\Delta E = 100$ eV, effective area ~ 500 cm^2). Section 4 presents a set of simulations with instruments of much higher spectral resolution (AXAF High Energy Transmission Gratings, HETG, $\Delta E = 1.5$ eV, collecting area ~ 100 cm^2, "AXAF Proposer's Guide", vs 1.0, 1997 [1] ; and Constellation-X baseline Calorimeter, $\Delta E = 3$ eV, collecting area $\sim 10,000$ cm^2, "The High Throughput X-ray Spectroscopy (HTXS) Mission", 1997 [2]). We finally present our conclusions in Section 5.

2. Models

We calculated the curves of growth of all the 268 permitted resonant absorption lines of C, O, Ne, Mg, Si, S and Fe, in the 0.1–10 keV energy range, with oscillator strengths greater than 0.05. **We used atomic data from the complete list of permitted LS-type (LS coupling transitions) resonant lines of all ionization states of 18 elements tabulated in Verner et al. (1996). Intercombination and**

[1] http://asc.harvard.edu/USG/docs/pg_c_ps.html

[2] http://constellation.gsfc.nasa.gov/documentation.html.

forbidden lines are not included in that compilation. We carried out the calculations considering the exact Voigt profile for the lines, i.e. considering both Doppler and natural broadening. As suggested by the width of the absorption lines detected in the UV spectra of the UV/X-ray ionized absorbers (Mathur et al. 1994, 1995, 1997, 1998), in addition to the thermal Doppler broadening we consider here a term accounting for gas turbulence, and refer to this term as the "turbulence velocity" σ_v along the line of sight.

We calculated spectra emerging from photoionized gas for a number of values of N_H, U, and σ_v. Relative ionic abundances and edge-like absorption features for given U and N_H and for a particular shape of the nuclear ionizing continuum are those calculated by CLOUDY (Ferland, 1997, vs 90.04), while the intensity and profile of the resonance absorption lines are consistently computed here for a given value of σ_v. The result is an emerging spectrum including both absorption edges and lines.

We considered only line absorption, not emission. **We used CLOUDY (vs 90.04, Ferland, 1997) to build total (transmitted + emitted) spectra and verified that, for the range of total column densities and ionization parameters considered here, this assumption corresponds (for a spherical configuration) to covering factors $f_c < 0.1$ (in good agreement with the Netzer, 1993, results: see his Fig. 3). In an ideal optically thin case, in which (a) the ionized gas isotropically and uniformely covers the central source ($f_c = 1$), (b) any systematic (inflowing or outflowing) motion of the gas is absent, and (c) any line destruction mechanism (autoionization, Compton scattering, photoabsorption) is inefficient, then scattering of the resonant emission line photons in the line of sight would exactly compensate for the line absorption along the line of sight, and, according to Netzer (1996), only emission features (mainly recombination lines) would be present in the total spectra. Any deviation from the above ideal condition would produce net absorption lines, which can therefore diagnose the physical and geometrical conditions of the absorbing material.** Presence of outflows instead would imply that both emission and absorption lines are present in the emergent spectra, with the absorption lines blueshifted with respect to the emission ones. In this paper, however, for the sake of simplicity we assume that a cloud of gas with negligible covering factor ($f_c < 0.1$) is completely obscuring the line of sight, and therefore that the contribution from emission lines to the overall spectrum is negligible. In comparing our model with real spectra it must be taken in mind that absorption lines may be partly compensated by line scattering **and recombination lines** for significant covering factors, or that emission lines may appear redwards (bluewards) of the absorption lines if the matter is outflowing (inflowing).

In the next paragraph we present the details of the computation, and show some examples of both growth curves and emerging spectra.

2.1. Computation

The equivalent width of a resonant absorption line is:

$$\mathrm{EW} = \int_0^{+\infty} \left[1 - e^{-\tau_\nu}\right] d\nu, \tag{1}$$

where τ_ν is the dimensionless specific optical depth of the considered transition:

$$\tau_\nu = \int_0^L ds \alpha_\nu = n_l L \frac{\pi e^2}{mc} f_{lu} \Phi(\nu). \tag{2}$$

In the above equation α_ν is the absorption coefficient at the frequency ν in cm^{-1}, n_l is the number density of ions of the given element which populate the **l**ower level in the unit volume (in cm^{-3}), L is the linear dimension of the cloud of gas along the line of sight (in cm), f_{lu} is the oscillator strength of the electron transition from the **l**ower to the **u**pper level, m is the electron mass in g, and $\Phi(\nu)$ is the normalized Voigt profile. With these units the equivalent width in equation (1) is in Hz. The Voigt profile can be written as (e.g. Rybicky & Lightman 1979):

$$\Phi(\nu) = \frac{1}{\sqrt{\pi}\Delta\nu_D} H(a,u), \tag{3}$$

where $H(a,u)$ is the Voigt function:

$$H(a,u) = \frac{a}{\pi} \int_{-\infty}^{+\infty} \frac{e^{-y^2} dy}{a^2 + (u-y)^2}. \tag{4}$$

In equation (4) a is essentially the ratio between the natural and the Doppler line widths Γ and $\Delta\nu_D$, and $u = (\nu - \nu_0)/\Delta\nu_D$. For small values of a the center of the line is dominated by the Doppler profile, while the wings are dominated by the lorentzian profile. As is well known, this influences the growth curves making them increasing with N_H even over the core saturation.

We consider two different contributions to the Doppler profile: (a) the thermal motion of the ions, and (b) the dispersion velocity σ_v of the gas along the line of sight:

$$\Delta\nu_D = \frac{\nu_0}{c} \left(\frac{2kT}{M} + \sigma_v^2 \right)^{0.5}. \tag{5}$$

Let us estimate the relative contribution of the two terms in equation (5):

$$\frac{v^{therm}}{\sigma_v} = \frac{\sqrt[2]{2kT}}{\sqrt[2]{m}\sigma_v} \simeq 1.3 \frac{(T)_6^{0.5} A^{-0.5}}{(\sigma_v)_{100}}. \tag{6}$$

In equation (6) $(T)_6$ is the equilibrium temperature of the gas in units of 10^6 K, $(\sigma_v)_{100}$ is the dispersion velocity in units of 100 km s^{-1}, and A is the atomic weight of the considered element. For a highly ionized gas in photoionization equilibrium, the temperature spans the range $(T)_6 \sim 0.1 - 1$. In a such a gas the elements lighter than O-Ne are usually fully stripped (the threshold element over which bound ions are still present depending strongly on the photoionizing continuum shape), and so the residual opacity from both bound–free and bound-bound transitions is mainly due to the heavy elements (from O to Fe). Assuming therefore $(T)_6 = 0.5$, $(\sigma_v)_{100} = 1$, and A=16 (the atomic weight of the lightest non-fully stripped element), we get, from equation (6), $v^{therm}/\sigma_v \simeq 0.2$. For the iron ions (A=56) we would find $v^{therm}/\sigma_v \simeq 0.1$. Hence, for dispersion velocities of ~ 100 km s^{-1}, the contribution of the thermal motion of the ions to the broadening of the absorption line is only $\sim 10 - 20\%$ of the total, and it decreases linearly with increasing σ_v. Therefore, the second term in equation (5) is the dominant one for $(\sigma_v)_{100} \gtrsim 1$.

2.2. Growth Curves:

Fig 1 and 2 show the growth curves of the Kα and Kβ lines of H-like and He-like C, O, Ne and Fe, for (a) $\sigma_v = 0$ (Doppler broadening entirely due to the thermal motion of the ions), and (b) $\sigma_v = 1000$ km s^{-1} respectively. The equivalent widths of the two Kα lines of H-like ions have been summed to give a single equivalent width for the doublet. The ionization state of the absorbing gas is that of a typical flat X-ray spectrum, broad optical emission line type 1 AGN 'warm absorber' (LogU=1) for C, O, and Ne, while a much higher ionization case (LogU=3) is adopted for the FeXXV and FeXXVI lines. In both cases the ionizing continuum used is the 'AGN Spectral Energy Distribution' (SED), tabulated in CLOUDY (Ferland, 1997, vs. 90.04). However, we stress that the growth curves depend only on the relative abundance of the ion under investigations, and not on the particular combination of U and shape of the ionizing continuum producing this abundance.

At low column densities ($\lesssim 10^{21-23}$ cm^2: the exact value depending on the considered line and dispersion velocity), the equivalent width of each line increases linearly with N_H. For higher values of N_H the optical depth of the line core saturates and the lorentzian profile begins to drive the further slower growth of the equivalent width with increasing columns. The linear branch of the growth curves (the low column density limit) is described by equation (1) in the limit $\tau_\nu << 1$:

$$\mathrm{EW} \simeq \int_0^{+\infty} d\nu \tau_\nu = n_l L \frac{\pi e^2}{mc} f_{lu} = \tau_{tot}. \quad (7)$$

Let us define A_X, ξ_{X^i} and N_H as the abundance of the element X relatively to the H abundance, the

relative abundance of the ion i of the element X, and the equivalent hydrogen column density along the line of sight respectively. With these positions and introducing an appropriate numerical format we have:

$$\mathrm{EW} \simeq 2.2(\xi_{X^i})_{0.4}(A_X)_{-5}(\mathrm{N}_H)_{22}(f_{lu})_{0.5}\ \mathrm{eV}. \tag{8}$$

When the core of the line becomes opaque to the radiation, equation (8) is no longer valid, and the computation of the equivalent width must be carried out using equation (1) with the exact shape of the profile function. A comparison between the curves in Fig. 1 and those in Fig. 2 allows to evaluate the effects of the line profile upon the resulting equivalent width. When the Doppler broadening is dominated by the thermal motion of the ions ($\sigma_v << 100$ km s^{-1}, Fig. 1), the dynamical range of variation of the equivalent width of each line with increasing N_H is much smaller than in the case in which the Doppler broadening is dominated by a high dispersion velocity of the gas along the line of sight ($\sigma_v \gtrsim 100$ km s^{-1}). This is because when the line is strongly broadened the core of the line needs larger column of gas to become optically thick, and so the linear branch of the growth curves spans over a larger range of N_H before saturating. From equations (2), (3) and (5), using the same numerical factor as in equation (8), and setting $\beta_{\sigma_v} = \sigma_v/c$, we get:

$$\tau_0 \simeq 2.9(f_{lu})_{0.5}(\xi_{X^i})_{0.4}(A_X)_{-5}A^{0.5}(\mathrm{N}_H)_{22}\left[(T)_6 + A(2.3\times10^3\beta_{\sigma_v})^2\right]^{-0.5}E_0^{-1}. \tag{9}$$

In the above equation the two terms within the square brackets describe the contribution to the core optical depth by the two considered Doppler mechanisms. From equation (6) we know that dispersion velocities of the gas along the line of sight greater than ~ 100 km s^{-1} make the turbulence broadening mechanism very efficient compared to the thermal one, and so reduce the core optical depth of each line. Equation (9) allows then to define and evaluate the core optical depth in the two extreme cases: $\sigma_v = 0$ (thermal motion only: τ_0^{therm}) and $\sigma_v \gg \sqrt{kT/M}$. We get:

$$\tau_0^{therm} \simeq 2.9(f_{lu})_{0.5}(\xi_{X^i})_{0.4}(A_X)_{-5}A^{0.5}(\mathrm{N}_H)_{22}(T)_6^{-0.5}E_0^{-1}, \tag{10}$$

$$\tau_0^{turb} \simeq 1.24(f_{lu})_{0.5}(\xi_{X^i})_{0.4}(A_X)_{-5}(\mathrm{N}_H)_{22}(\beta_{\sigma_v})_{-3}^{-1}E_0^{-1}. \tag{11}$$

The ratio between these two quantities does not depend on the particular considered transition, the distribution of the ionic abundances in the gas, and its column density, and is therefore a good estimator of the relative contribution of the two Doppler broadening mechanisms to the core optical depth:

$$\frac{\tau_0^{therm}}{\tau_0^{turb}} = 2.3A^{0.5}(T)_6^{-0.5}(\beta_{\sigma_v})_{-3}. \tag{12}$$

Equation (12) tells us that a given column of non-turbulent highly ionized gas in photoionization equilibrium can be more than a factor 10 thicker to the resonant absorption process (at the energy of the transition) than an identical column of gas undergoing strong turbulence ($\sigma_v \gtrsim 300$ km s^{-1}, i.e. $(\beta_{\sigma_v})_{-3} \gtrsim 1$).

2.3. Emerging X-ray Spectra:

The relative importance of the spectral features in spectra emerging from photoionized gas obscuring the line of sight strongly depends on the Spectral Energy Distribution of the ionizing continuum in the UV to X-ray energy range. We therefore treat separately the two extreme observed cases: (a) flat X-ray spectrum, broad optical emission line type 1 AGN continua, and (b) steep X-ray spectrum, narrow optical emission line type 1 AGN continua. **If a peculiar class of AGN does exists, with intrinsic UV to X-ray continuum switching between these two extreme observed cases (as suggested by the behaviour observed in 1H 0419-577, NGC 4051, RE J2248-511: Guainazzi et al. 1998a,b, Turner et al 1998, Puchnarewicz et al., 1995) then sources belonging to this class would show emerging spectra of the types (a) and (b) alternately.**

2.3.1. Flat X-ray Ionizing Continuum

Typical O-UV to X-ray continua of broad line type 1 AGN (i.e. $\alpha_E \sim 1$, $\alpha_{OX} \sim 1.3$) transmitted by photoionized gas show deep OVII-OVIII edges, as those are, usually, the most abundant oxygen ions. In these conditions, when the Oxygen is mainly distributed in highly ionized states, Carbon is almost fully stripped and Neon is mostly distributed between NeIX-XI. Conversely high ionization Iron ions are not much populated, the main ions being FeXIV-XX (Nicastro et al., 1998a). In Fig. 3, we show 0.1–5 keV spectra emerging from an outflowing wind photoionized by a typical flat X-ray spectrum, broad optical emission line type 1 AGN continuum (Ferland, 1997), for three different values of LogU= $0.5, 1, 1.5$. We used an outflowing velocity of $v_{out} = 1000$ km s^{-1}, which is typical for the UV outflowing component in 'warm absorbers' (Mathur et al., 1995), and which corresponds to z $= -0.003$. For the dispersion velocity, we adopted a value $\sigma_v = 500$, km s^{-1}. The column of photoionized gas along the line of sight is fixed at $N_H = 6 \times 10^{21}$ cm^{-2}, which is the mean value in the Reynolds (1997) sample. We also added absorption from cold gas of column $N_H^{Cold} = 3 \times 10^{20}$ cm^{-2} to simulate a typical Galactic absorption along the line of sight. In each panel of Fig. 3 we plot the transmitted spectra corresponding to a given value of LogU.

Moving from LogU=0.5 to LogU=1.5 (i.e. from low to high ionization, from the upper to the lower panel of Fig. 3) the OVII K edge opacity decreases, due to the decreasing of the OVII/OVIII relative abundances ratio. Conversely the optical depth of the OVIII K edges increases until the OVII → OVIII photoionization rate becomes lower than the OVIII → OIX one. In the lower panel of Fig. 3 (LogU=1.5) only the OVIII K edge is visible, while the gas is almost completely transparent at the OVII K edge energy. In the lower ionization case (LogU=0.5: upper panel of Fig. 3), a deep OVII K edge is instead present, along with the 0.49 keV K edge of CVI. NeIX K edge is marginally visible because of the low column density adopted.

Strong OVII Kα and Kβ and OVIII $K\alpha$ resonance absorption lines at 0.574, 0.653, and 0.665 keV respectively, as well as CV, CVI and NeIX, NeX Kα and Kβ lines are present in these spectra with intensities and equivalent widths depending weakly on the ionization state. On the other hand, intensities and equivalent widths strongly depend on the dynamics of the absorbing clouds of gas along the line of sight, and on its column density. For the case under consideration ($\sigma_v = 500$ km s^{-1}, $N_H = 6 \times 10^{21}$ cm^{-2}) the equivalent widths of Kα and Kβ He-like and H-like Carbon, Oxygen and Neon are in the range 2-8 eV. In the medium and higher ionization cases, Kα and Kβ lines from Mg and Si are also present, along with two complex systems of SXI-SXV, and FeXV-FeXX L lines around 0.3 and 1 keV respectively. Their equivalent widths in the higher ionization case are of the order of 1 eV for each line. We note that the energies of the strong Kα and Kβ NeIX, NeX lines, as well as those of a number of FeXVII, FeXVIII lines, are all close to each other and to the energy of the OVIII K edge. Caution should then be made when fitting low-medium resolution spectra of 'warm absorbers' with a phenomenological multi-edge model. Neglecting the presence of this system of absorption lines (which may reach total equivalent width of up to a few tens of eV for $\sigma_v = 1000$ km s^{-1}), and leaving the optical depths of each edge free to vary independently in these fits, may result in good fits, from the χ^2 point of view, but in overestimating the OVIII optical depths.

2.3.2. Steep X-ray ionizing continuum

When the ionizing continuum is steep below 2 keV ($\alpha_E \gtrsim 2$) and flattens above this energy to $\alpha_E \sim 0.7 - 1.5$, as in many NLSy1, the resulting ionization structure can be quite different from the ones described in the previous section. In fact, in these condition C, O, and Ne would be almost fully stripped in the gas, while Iron would still be distributed in medium–low ionization states, giving rise to emerging spectra with no sharp absorption features below ~ 1 keV and a broad absorption structure between 1 and

2 keV due to a complex mixture of L resonance absorption lines and edges from FeX-FeXX.

As an example, fig. 4 shows two spectra emerging from an outflowing wind photoionized by a typical NLSy1 continuum (see Leighly et al., 1997), consisting of a black body with kT=0.13 keV, and a power law with $\alpha_E = 0.9$. **The relative normalization between the soft and the hard components is such that the ratio between the bolometric luminosity of the black body component and the 2-10 keV luminosity is** $(L_{Bol}(BB)/L_{2-10}(PL)) \simeq 10$ **(a mean value in the Leighly et al. sample).** We assume also in this case $v_{out} = 1000$ km s^{-1}, $\sigma_v = 500$ km s^{-1}, and a column of $N_H^{Cold} = 3 \times 10^{20}$ cm^{-2} neutral gas to mimic a typical Galactic absorption. In the upper panel of Fig. 4 we plot the spectrum emerging from gas with LogU=-0.5 and LogN_H=22. Both absorption lines and edges form the H-like and He-like ions of C, O and Ne, along with a number of Si L lines around 0.3 keV, are imprinted on spectra emerging from photoionized gas with this (or lower) value of U, similarly to what is found in the case of flat X-ray ionizing continuum, see figure 3. The lower panel of Fig. 4 illustrates the case of a much higher ionization (LogU=1). Here we use a column density an order of magnitude higher than in the previous case, to highlight the peculiarities of this model: no deep absorption edge is visible in this spectrum, despite of the very high column of $N_H = 10^{23}$ cm^{-2}, while a complex system of strong absorption lines between 1 and 2 keV is clearly visible, due to almost 60 L lines of mid-ionized Iron, and Kα and Kβ lines of Mg, Si and S. The iron L lines around 1 keV are all very close in energy and their equivalent widths span from a few eV, for $\sigma_v = 500$ km s^{-1}, up to tens of eV for $\sigma_v = 1000$ km s^{-1}. The total equivalent width due to these lines between 1 and 1.5 keV can be as high as of few hundreds of eV.

Let us now suppose that the ionized gas in NLSy1 has physical properties similar to the 'warm absorbers' in flat X-ray spectrum type 1 AGN, i.e. similar electron density and similar distance from the source of the ionizing radiation in units of gravitational radii. Pounds et al. (1995) and Laor et al. (1997) suggested that steep X-ray spectrum, narrow line quasars are emitting close to the Eddington luminosity, at a rate, say, a factor of ten higher than flat X-ray spectrum broad line quasars. This means that the black hole mass of steep X-ray quasars is a factor of ten smaller than that of flat X-ray quasars with a similar luminosity (in agreement with variability studies, Fiore et al. 1998b, and with detailed modeling of the optical-UV-X-ray SED of NLSy1, Puchnarewicz et al 1998, Siemiginowska et al 1998). **The remarkable uniformity of ionization parameters found by Reynolds (1997) and George et al. (1998), in their samples of Seyfert 1 galaxies and quasars of luminosity spanning three orders of magnitude implies that the product** $R^2 n_e$ **scales linearly with the luminosity in these objects. If this correlation holds for NLSy1 too, then we can estimate the** $R^2 n_e$ **factor of a NLSy1 of a**

given luminosity using, for example, the Reynolds estimate but scaling the distance between the absorber and the ionizing source by the above factor of ten. For a NLSy1 of luminosity 10^{43} erg s^{-1} we find $R^2 n_e \sim 10^{40}$ cm^{-1}, using the typical ionization parameter found by Reynolds (1997). Using this value, and the correct ionizing continua, we expect for a typical NLSy1 a LogU of 0.8-1.2, and therefore a spectrum similar to that plotted in the lower panel of Fig. 4.

3. Data and Simulations

To compare our models with the available data and to make predictions on what we will be able to observe with the next generation of X-ray spectrometers (i.e. gratings and calorimeters), we folded our photoelectric+resonant absorption model with the responses of the ASCA SIS, AXAF ACIS/HETG, and a high resolution, high effective area calorimeter as the baseline for the future mission Constellation-X. The simulations were performed using model parameters as deduced from the ASCA data of the Seyfert 1 galaxy NGC 985, and the NLSy1 IRAS 13224-3809. We discuss these two cases in turn.

3.1. Flat ionizing continuum: The case of NGC 985

NGC 985 is a Seyfert 1 galaxy known to host an ionized absorber (Brandt et al 1994). Nicastro et al. (1998b) observed the source with ASCA and confirmed the presence of an ionized absorber along the line of sight. They find that a single-zone photoionization model (accounting for photoelectric absorption only, model *a*) is not able to explain completely the complex absorption structure seen in the ASCA spectrum (the continumm has been parameterized as a power law with $\alpha_E = 1.3$ up to 2.3 keV, while above this energy the spectrum flattens by $\Delta\alpha_E = 0.6$, the ionized absorber parameters are LogU=0.93 ± 0.09, LogN$_H = 21.95 \pm 0.05$, and z$_{abs} = 0.023^{+0.034}_{-0.029}$, which implies a maximum outflowing velocity $\approx 15,000$ km s^{-1}). Analysis of the ASCA SIS residuals shows a significant deficit of counts around ~ 1 keV (figure 5a). The equivalent width of this feature (estimated by adding a gaussian absorption line to the continuum model) is of -(13 ± 4.0) eV.

We computed the spectrum emerging from gas photoionized by the NGC 985 optical to X-ray continuum using our photoelectric+resonant absorption model. We extrapolated the soft X-ray power law, as measured from the ASCA data, through optical wavelengths. This is consistent with both the measured O-UV spectral index $\alpha_{O-UV} = 1.4$ (De Vaucouleurs et al., 1991) and α_{OX}=1.4. We adopted for LogU

and LogN_H the best fit values given above and an outflowing velocity of 1000 km s^{-1}, which is the mean measured value for the known O-UV/X-ray ionized absorbers (Mathur et al., 1994, 1995, 1997, 1998), and is consistent with the estimate of the 'warm absorber' redshift in this source. We used a dispersion velocity of 1000 km s^{-1}. The model is plotted in figure 5c. It shows strong resonance absorption lines between 0.85 and 1.2 keV due to the redshifted Kα and Kβ NeIX and Kα NeX lines. The blend of these three lines has a total equivalent with of about 20 eV, similar to the equivalent width of the line feature in figure 5a. We folded this model with the ASCA–SIS response, and simulated a 40 ksec observation of NGC 985. We fitted the resulting spectrum with model *a*). The ratio between the simulation and best fit model *a*) is shown in figure 5b: it resembles strikingly the residuals to the 'real' spectrum in figure 5a. While this is certainly not a self consistent, quantitative and unique description of the spectrum of NGC 985, it indicates that resonant absoprtion may well be cause of the feature observed at about 1 keV.

The spectrum in figure 5c also shows strong absorption Kα and Kβ lines from OVII and OVIII at 0.57 and 0.65 keV. There is no evidence for an absorption feature (in addition to photoelectric absorption) at these energies in the ASCA spectrum of NGC 985 (Fig. 5a). Contribution from emission lines due to recombination could be important at these energy, and so they could help in reducing the depth of the absorption lines. Line emission strongly depends on the covering factor and therefore an accurate estimate of line emission intensity can provide information on the geometry and distribution of the ionized gas. However, the above energy is close to the lower threshold of the SIS instrument, where the calibration is most uncertain and problems due to the Residual Dark Distribution (RDD) are large, and where the CCD energy resolution is of 5-6 only. For a quantitative study of the OVII and OVIII emission/absorption lines we should await instruments with better energy resolution and coverage.

As a next step we folded the photoelectric+resonant absorption model of figure 5c with the responses of AXAF ACIS/HETG and the baseline Constellation-X calorimeter, which has a factor of 2 worse energy resolution but a factor of 100 higher effective area (at 1 keV). The simulations are shown in figures 6a,b,c and 7a,b,c for three different values of the dispersion velocity: σ_v = 100, 500 and 1000 km s^{-1} for panels a,b and c respectively. The first order AXAF ACIS/MEG ("Medium Energy Grating") simulations (figure 6) were performed using the MARX simulator (Wise et al., 1997, "MARX User Guide", vs 1.0) [3]). The exposure time is of 80 ksec. To simulate the calorimeter spectrum (figure 7), we wrote a simple

[3]http://asc.harvard.edu/prop_port.html#marker_marx

program to fold our models with the response matrix [4] and add statistical noise. The exposure time in the Constellation-X calorimeter simulations is of 10 ksec.

Resonance absorption lines of width $\gtrsim$200 km s^{-1} are detected in the AXAF ACIS/HETG first order spectrum. All the strongest lines in figure 5c are resolved in the spectra of figure 6b,c. AXAF HETG spectra of Seyfert 1 galaxies will then establish whether resonant absorption is important in the ionizing gas and then provide estimates of the gas dispersion velocity and bulk motion. This will allow to solve unambiguously the open and controversial issue on the identification between the X-ray and the UV ionized absorbers. However, the signal to noise will be poor in most cases: the OVIIIKα/Kβ and NeIX Kα/Kβ line ratios, which can be used for plasma diagnostic, cannot be estimated with uncertainty $\lesssim$100%; line widths and profiles, which gives information on the geometrical and dynamical configuration of the absorber can be roughly measured but not studied in detail. The HETG can obtain spectra of comparable quality for about one hundred AGN.

The large effective area of the Constellation-X calorimeter along with a good energy resolution will permit to obtain high signal to noise spectra, of quality similar to optical spectra of AGNs, of sources of the brightness of NGC 985 . This will allow to apply plasma diagnostics, measure accurately both the chemical composition and ionic distribution of the gas, discriminate between collisional ionization and photoionization, and study the time-evolving behaviour of the relevant physical quantities (temperature, relative ionic abundances, etc.) which will allow in turn to constrain important physical and geometrical parameters (electron density, and radial distance: Nicastro et al., 1998a). The Constellation-X calorimeter could provide moderate signal to noise spectra, similar to those in figure 6, of sources down to a flux limit of a few 10^{-13} erg cm^{-2} s^{-1}, which increases the sample of possible targets to a few tens of thousands sources. AGNs with luminosity in the range 10^{43-44} erg s^{-1} can be studied up to z=0.3-0.5, while more luminous (10^{46-47} erg s^{-1}) quasars will be available up to z$\sim$ 3 (the limit is given by the bandwidth of the Constellation calorimeter more than by its sensitivity, since features at 0.5-1 keV are redshifted to 0.12-0.25 keV for z=3). This will permit to study the evolution of physical state, chemical composition, and geometry of the absorbing gas with redshift and luminosity. Statistical studies on the distribution of the absorber density, ionization state, chemical composition and distance from the ionizing source will be possible, which can give information on the absorber origin.

[4] ftp://legacy.gsfc.nasa.gov/htxs/calor.rsp

3.2. Steep Ionizing Continuum: the Case of IRAS 13224-3809

We choose to test our model on the NLSy1 galaxy IRAS 13224-3809, which showed in an ASCA observation a deep absorption feature in the interval 1-2 keV, interpreted by Leighly et al. (1997) in terms of resonant absorption from gas outflowing with v/c$\sim$ 0.5

Figure 8a shows the ratio between the coadded ASCA SIS0 and SIS1 data and the best fitting model composed by a black body plus a power law, with best fit parameters given by kT=0.134 keV, $\alpha_E = 1.16$ **and** $(L_{Bol}(BB)/L_{2-10}(PL)) = 9.8$ **(fully consistent with both the Leighly et al, 1997, and the Hayashida et al., 1997, estimates).** A deep and broad deficit of counts is evident between 0.9 and 2 keV (also see figure 1 in Leighly et al. 1997). The absorption feature equivalent width (estimated by adding a gaussian absorption line to the continuum model) is large: EW=-(180 ± 30) eV. **We note that, even if the deficit of counts occurs approximately where the black body and the power law components match each other, we were not able to model the absorption–like feature without invoking a third component.**

We computed the spectrum emerging from gas photoionized by the IRAS 13224-3809 UV to X-ray continuum for a number of values of LogU (from -0.5 to 1.5), LogN$_H$ (from 10^{22} to 10^{24} cm^{-2}) and σ_v (from 100 to 1000 km s^{-1}). We extrapolated down to 13.6 eV and up to to **100 keV** the best fit continuum to the ASCA data of IRAS 13224-3809. This is in good agreement with the optical UV to X-ray measures of this source which suggest that the thermal disk component in this object could be present at higher energies than usually found in soft X-ray flat, broad line type 1 AGN (Mas-Hesse et al., 1994). **We adopted, for the hard X-ray power law, the best fit spectral index** $\alpha_E = 1.16$**. This value is in excellent agreement with the mean estimate of Hayashida et al. (1997). However, as Brandt, Mathur & Elvis (1997) pointed out, the spectral index of the hard power law of IRAS 13224-3809 is highly variable, ranging between 0.7 and 1.3. The value that we used in our model represents therefore only a mean value. We stress however that the exact shape of the hard power law does not affect strongly the distribution of the relative ionic abundances in the gas for elements lighter than Neon, which is instead mainly driven by the presence of a strong soft excess below** ~ 2 **keV. Our results are therefore rather insensitive to the exact slope of the hard power law.** As in the previous case we adopted an outflowing velocity of 1000 km s^{-1}. We folded these models with the ASCA-SIS response and then fitted them with a black body plus power law model. As an example figure 8b shows the ratio between an 80 ksec simulation obtained using logN_H=23.5, LogU=1

and outflowing and dispersion velocities of 1000 km s^{-1} (model shown in figure 8c), and the best fitting black body plus power law model. **We note that all the relevant absorption lines lie in a spectral region in which the intrinsic continuum is still dominated by the soft black body component (Fig 8c, but see also Fig. 4).** The residuals resemble those in figure 8a. The large deficit of counts between 0.9 and 2 keV is due to the presence of a large number of iron L lines. The coadded equivalent width of these lines is about 130 eV, similar to the equivalent width of the absorption feature in figure 8a.

As for the case of NGC 985, we plot in figure 9a,b,c and 10a,b,c three simulations obtained convolving the spectrum in figure 8c with the AXAF/MEG and Constellation-X calorimeter responses. The simulations are shown for three values of the dispersion velocity, σ_v = 100, 500 and 1000 km s^{-1} (figure a, b and c respectively). Integration time was 100 ksec for the first order AXAF/MEG spectrum and 20 ksec for the Constellation-X calorimeter spectrum.

Many single Fe L lines are well resolved even in spectra with dispersion velocity of 1000 km s^{-1}. AXAF/HETG spectra of low redshift NLSy1 with luminosity L= $10^{43} - 10^{44}$ erg s^{-1} will permit to unambiguously establish whether an ionized absorber is indeed responsible for the 1 keV deficit of counts seen in many moderate resolution X-ray spectra of these sources. The low signal to noise ratio of AXAF/HETG spectra, however, will not allow to apply plasma diagnostics to infer the physical properties of the absorbers. Nevertheless the outflowing and dispersion velocities of the gas will be accurately derived, as well as the relative Ne to O, and Fe to Si and Mg abundances, which will put important constraints on the geometry and the chemical composition in the AGN environment. The high effective area of the Constellation-X calorimeter will allow to greatly increase the sample of narrow-line type 1 AGN observed at high resolution. The complex Iron L edges and lines absorption system could be detected in high luminosity narrow line quasars up to redshift $\lesssim 2$, or even higher, depending on the actual response below the carbon edge (0.283 keV), while Mg and Si Kα and Kβ resonance absorption lines could be detected up to z$\sim$ 3. The good energy resolution (3 eV), will permit to separate the strongest (oscillator strength greater than 0.05) single resonance absorption lines of the 1 keV Iron L edge+line complex, so allowing for a clear diagnostic of the mechanism responsible for the ionization of the gas. In particular, an accurate measure of the relative abundances of the very stable FeXVII Li-like ion could allow to clearly distinguish between gas in collisional or photoionization equilibrium (Nicastro et al. 1998a). Time evolving ionization can also be investigated, so giving constraints on the electron density and the radial distance of the absorbers (Nicastro et al. 1998a).

4. Conclusions

We have calculated spectra emerging from ionized gas taking into account both photoelectric and resonant absorption. We find that the emerging spectra are strongly modified by resonant absorption if the dispersion velocity in the gas is $\gtrsim$100 km s^{-1}. This or even higher values are not irrealistic, since many broad line AGN show absorption lines in the UV blueshifted by 200-2000 km s^{-1}, and broadened by similar dispersion velocities.

In particular we find:

1. The distribution of relative ionic abundances in photoionized gas dramatically depends on the exact shape of the ionizing continuum.

2. Strong Kα and Kβ resonance absorption lines from He-like and H-like ions of C, O, and Ne, along with deep CVI, OVII-OVIII, NeIX-X K edges, and FeXV-XVII L edges, are expected to be present in the 0.1-3 keV spectra of flat X-ray spectrum quasars emerging from photoionized gas along the line of sight. When fitting low and medium resolution X-ray data with phenomenological multi-edge models, these resonance absorption lines may produce the effect of overestimating the optical depth of the OVIII K edge.

3. Conversely, no strong absorption edge is expected to be imprinted on spectra emerging from gas illuminated by steep ionizing continua, with physical and geometrical properties similar to those found in broad line type 1 AGN. However, a large number of strong Fe L and Mg, Si, and S Kα and Kβ resonance absorption lines (almost 70) are predicted between 1 and 2 keV. Fitting low and medium energy resolution data with continuum models may then result in deep smooth negative residuals at these energies. We then suggest that the $\sim$ 1 keV absorption feature observed by ASCA in several Narrow Line Seyfert 1 galaxies can be explained in terms of resonance absorption lines, without requiring relativistic outflowing velocities of the gas.

4. The equivalent width of the predicted resonant absorption lines strongly depends on the column density of the absorbing gas and the its dispersion velocity. Assuming the range of N_H typically observed and dispersion velocities of 0–1000 km s^{-1}, we estimate equivalent widths spanning from a few eV to a few hundreds of eV.

F.F. acknowledges support from NASA grant NAG5-2476 and NAG5-3039.

REFERENCES

Boller Th., Brandt W.N., Fink H., 1996, A&A, 305, 53

Brandt W.N., Fabian A.C, Nandra K., Reynolds C.S., Brinkmann W., 1994, MNRAS, 271, 958

Brandt W.N., 1995, PhD Thesis, University of Cambridge (UK)

Brandt W.N., Mathur S., Elvis M., 1997, MNRAS, 285, L25

De Vacouleurs G., et al., 1991, RC3.9, vol. p

Ferland, 1997 CLOUDY vs. 90.04

Fiore F., Elvis M., McDowell J. C., Siemiginowska A., Wilkes B. J., 1994, ApJ, 431, 515

Fiore F. et al. 1998a, MNRAS, in press, astro-ph/9804256

Fiore F. et al. 1998b, ApJ, in press, astro-ph/9803248

George I.M., Turner T.J., Netzer H., Nandra K., Mushotzky R.F., & Yaqoob T., 1998, ApJS, 114, 73

Guainazzi M. et al, 1998a, MNRAS, in press astro-ph/9808009

Guainazzi M., Nicastro F., Fiore F. et al, 1998b, MNRAS, in press astro-ph/9807213

Hayashida K., 1997, in *Emission LIne in Active Galaxies: New Methods and Techniques*, Eds, B.M. Peterson, F.-Z. Cheng, A.S. Wilson, (San Francisco: ASP Press), p. 40

Kriss G.A., et al., 1996a, ApJ, 467, 629

Kriss G.A., Espey B.R., Krolik J.K., Tsvetanov Z., Zheng W., Davidsen A.F., 1996b, ApJ, 467, 622

Krolik J.H, Kriss G.A. 1995, ApJ, 447, 512 (erratum in 1996, ApJ, 456, 909)

Laor A., Fiore F. Elvis E., Wilkes B.J., McDowell J.C., 1997, ApJ, 477, 93

Leighly K.M., Mushotzky R.F., Nandra K., anf Foster K., 1997, ApJL, 489, 25

Mas-Hesse J.M., Rodriguez-Pascual, P.M., De Cordoba L., Sanz Fernandez, Boller Th., 1994, A&A, 283, 9

Mathur S., Wilkes B.J., Elvis M., Fiore F. 1994, ApJ, 434, 493

Mathur S., Elvis M., Wilkes B.J. 1995, ApJ, 452, 230

Mathur S., Wilkes B.J., Aldcroft T. 1997, ApJ. 478, 182

Mathur S., Wilkes B.J., Elvis M., 1998, ApJ, 503, 23

Matt G. 1994, MNRAS, 267, L17

Matt G., Brandt W.N., Fabian A.C. 1996, MNRAS, 280, 823

Matt G. et al. 1998, in preparation

Netzer H. 1993. ApJ, 411, 594

Netzer H. 1996, ApJ, 473, 781

Nicastro F., Fiore F., Perola G.C., Elvis M., 1998a, ApJ, in press, astro-ph/9808316

Nicastro F., Fiore F., Brandt W., Reynolds C., 1998b, *proceedings of the Symposium "The active X-ray sky"*, in press

Pfefferman E. et al. 1987, Proc. SPIE, 733, 519.

Pounds K.A., Done C., Osborne J.P., 1995, MNRAS, 277, L5

Puchnarewicz E.M., Branduardi-Raymond G., Mason K.O., Sekiguchi K., 1995, MNRAS, 276, 1281

Puchnarewicz E.M., Mason K.O., & Siemiginowska A., 1998, MNRAS, 293. 52

Reynolds C.S., 1997, MNRAS, 287, 513

Rybicky G.B. & Lightman A.P., 1979, *Radiative Processes in Astrophysics*, Jhon Wiley & sons, New York

Trümper J. 1983, Adv. Space Res., 2, No.4 241.

Turner et al., 1998, ApJ in press astro-ph/9807142

Verner, D. A., Verner, E. M., and Ferland, G. J., 1996, *Atomic Data Nucl. Data Tables*

Walter R., Fink H., 1993, A&A, 274, 105

Wise M.W., Davis J.E., Huenemoerder D.P., Houck J.C., Dewey D., Flanagan K.A., Baluta C., 1997, "MARX User Guide", vs 1.0

This manuscript was prepared with the AAS LaTeX macros v4.0.

Fig. 1.— Growth curves of the Kα and Kβ lines of H-like and He-like C, O, Ne and Fe, for $\sigma_v = 0$. The ionization state of the absorbing gas is that of a typical 'warm absorber' (LogU=1) for C, O, and Ne, and a much higher ionization case (LogU=3) for FeXXV and FeXXVI.

Fig. 2.— As Fig. 1, but for $\sigma_v = 1000$ km s^{-1}.

Fig. 3.— 0.1–5 keV spectra emerging from an outflowing wind photoionized by a typical flat X-ray, broad line type 1 AGN continuum, for LogU = 0.5, 1, 1.5, $v_{out} = 1000$ km s^{-1}, $\sigma_v = 500$ km s^{-1} and N$_H = 6 \times 10^{21}$ cm^{-2}. The low energy turn over is due to absorption from a column of neutral gas, to mimic typical Galactic absorption.

Fig. 4.— Spectra emerging from an outflowing wind photoionized by a typical NLSy1 continuum, and with $v_{out} = 1000$ km s^{-1} and $\sigma_v = 500$ km s^{-1}. The ionizing continuum used consists of a black body with kT=0.13 keV, and a power law with $\alpha_E = 0.9$. The ionization parameter and gas column density are LogU=-0.5, LogN_H=22, and LogU=1, Log$N_H = 23$ in the upper and lower panels respectively.

Fig. 5.— Ratio between the coadded ASCA SIS0 and SIS1 data of NGC985 and the best fitting model *a* (a). Ratio between a 40 ksec ASCA SIS simulation, obtained using the model plotted in the lower panel (see the text for details), and model *a* (b). The spectrum emerging from gas photoionized by the NGC 985 SED, when accounting for both photoelectric and resonant absorption (c). We adopted outflowing and dispersion velocities of 1000 km s^{-1}.

Fig. 6.— Simulations of 80 ksec 0.4–1.2 keV first order AXAF ACIS/MEG spectra of NGC 985. A dispersion velocity of $\sigma_v = 100$, 500 and 1000 km s^{-1} has been used in figure a), b) and c) respectively.

Fig. 7.— Simulations of 10 ksec spectra of NGC 985 taken with the Constellation-X calorimeter. A dispersion velocity of $\sigma_v = 100$, 500 and 1000 km s^{-1} has been used in figure a), b and c) respectively. The cut-off at low energy is partly due to the inclusion at low energy of neutral absorption from the Galactic column along the line of sight ($N_H = 3 \times 10^{20}$ cm^{-2}).

Fig. 8.— Ratio between the coadded ASCA SIS0 and SIS1 data of IRAS 13224-3809 and the best fitting black body plus power law model (a). Ratio between a 80 ksec ASCA SIS simulation, obtained using the model plotted in the lower panel (see the text for details) and the best fitting black body plus power law model (b). The spectrum emerging from gas photoionized by the IRAS 13224-3809 SED, when accounting for both photoelectric and resonant absorption (c). We adopted outflowing and dispersion velocities of 1000

km s^{-1}.

Fig. 9.— Simulations of 100 ksec 0.4-2 keV first order AXAF ACIS/MEG spectra of IRAS 13224-3809. A dispersion velocity of $\sigma_v = 100$, 500 and 1000 km s^{-1} has been used in figure a), b) and c) respectively.

Fig. 10.— Simulations of 20 ksec 0.3–2 keV spectra of IRAS 13224-2809 taken with the Constellation-X calorimeter. A dispersion velocity of $\sigma_v = 100$, 500 and 1000 km s^{-1} has been used in figure a), b) and c) respectively. The cut-off at low energy is partly due to the inclusion of neutral absorption from the Galactic column along the line of sight ($N_H = 4.8 \times 10^{20}$ cm^{-2}).

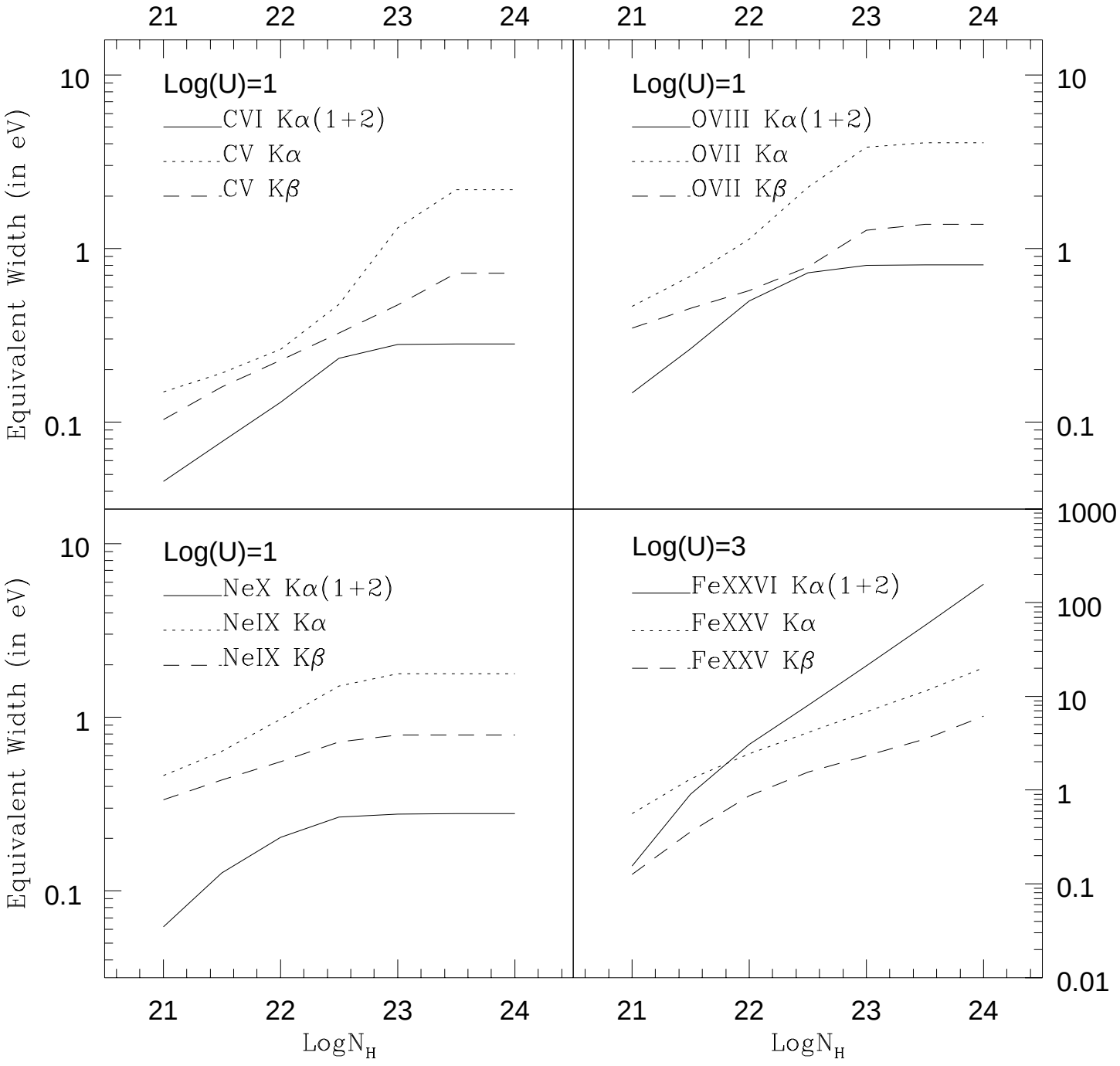
Log(U)=1
CVI Kα(1+2)
CV Kα
CV Kβ
Log(U)=1
OVIII Kα(1+2)
OVII Kα
OVII Kβ
Log(U)=1
NeX Kα(1+2)
NeIX Kα
NeIX Kβ
Log(U)=3
FeXXVI Kα(1+2)
FeXXV Kα
FeXXV Kβ
Equivalent Width (in eV)
Equivalent Width (in eV)
LogN$_H$
LogN$_H$
21
22
23
24
0.01
0.1
1
10
100
1000

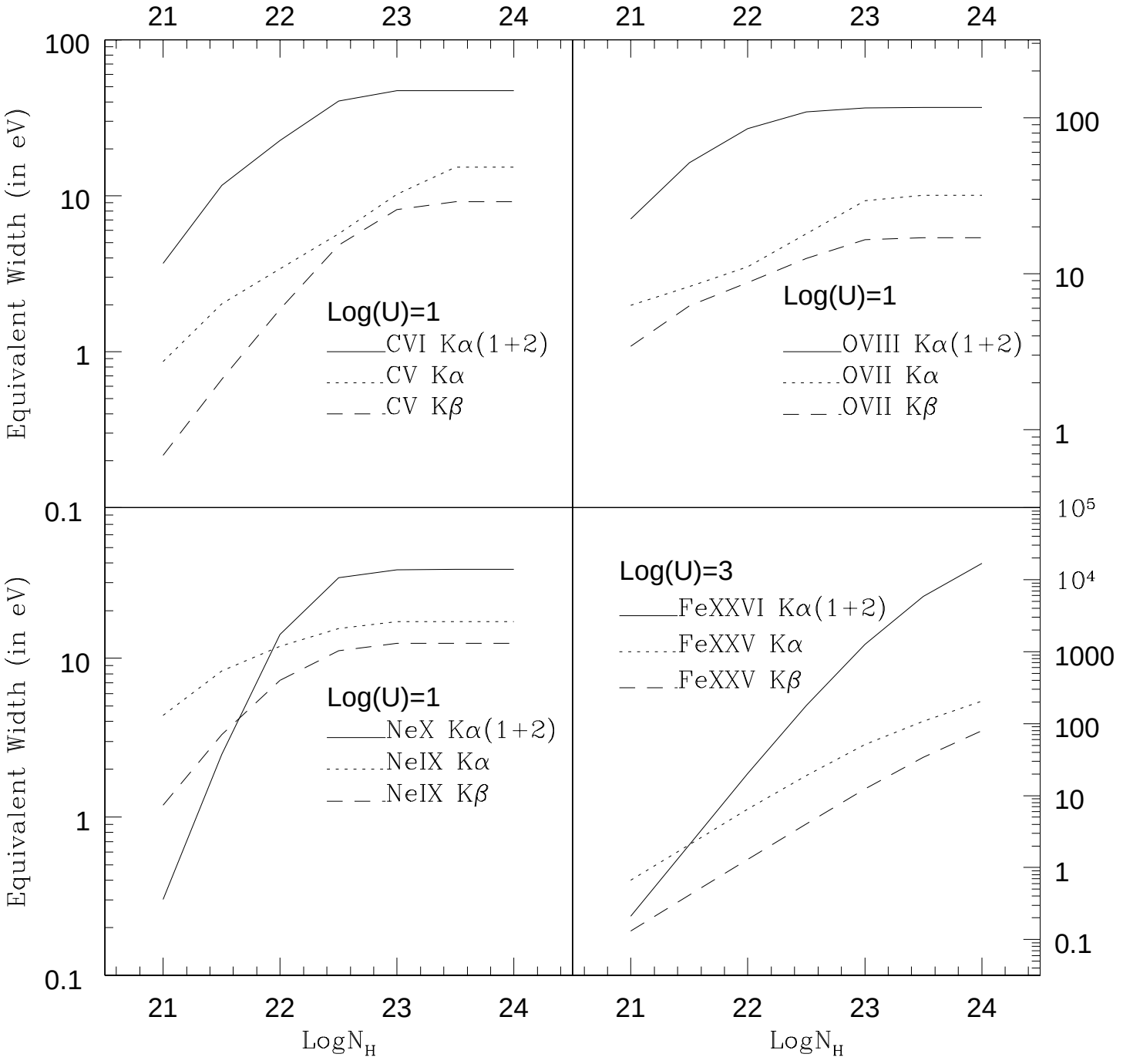
Log(U)=1
CVI Kα(1+2)
CV Kα
CV Kβ
Log(U)=1
OVIII Kα(1+2)
OVII Kα
OVII Kβ
Log(U)=1
NeX Kα(1+2)
NeIX Kα
NeIX Kβ
Log(U)=3
FeXXVI Kα(1+2)
FeXXV Kα
FeXXV Kβ
Equivalent Width (in eV)
Equivalent Width (in eV)
LogN$_H$
LogN$_H$
21
22
23
24
100
10
1
0.1
10^5
10^4
1000

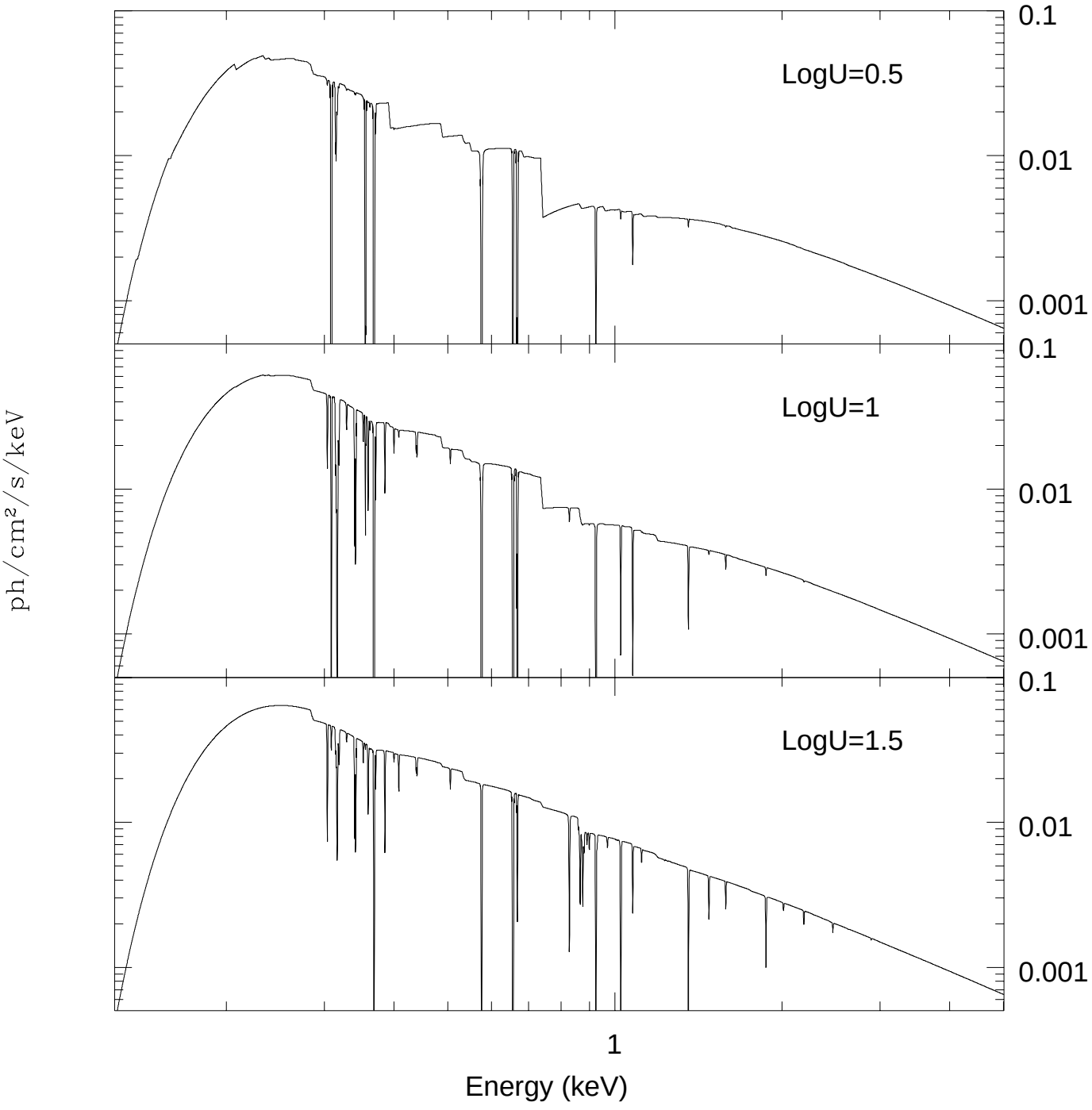
LogU=0.5
LogU=1
LogU=1.5
0.1
0.01
0.001
ph/cm²/s/keV
1
Energy (keV)

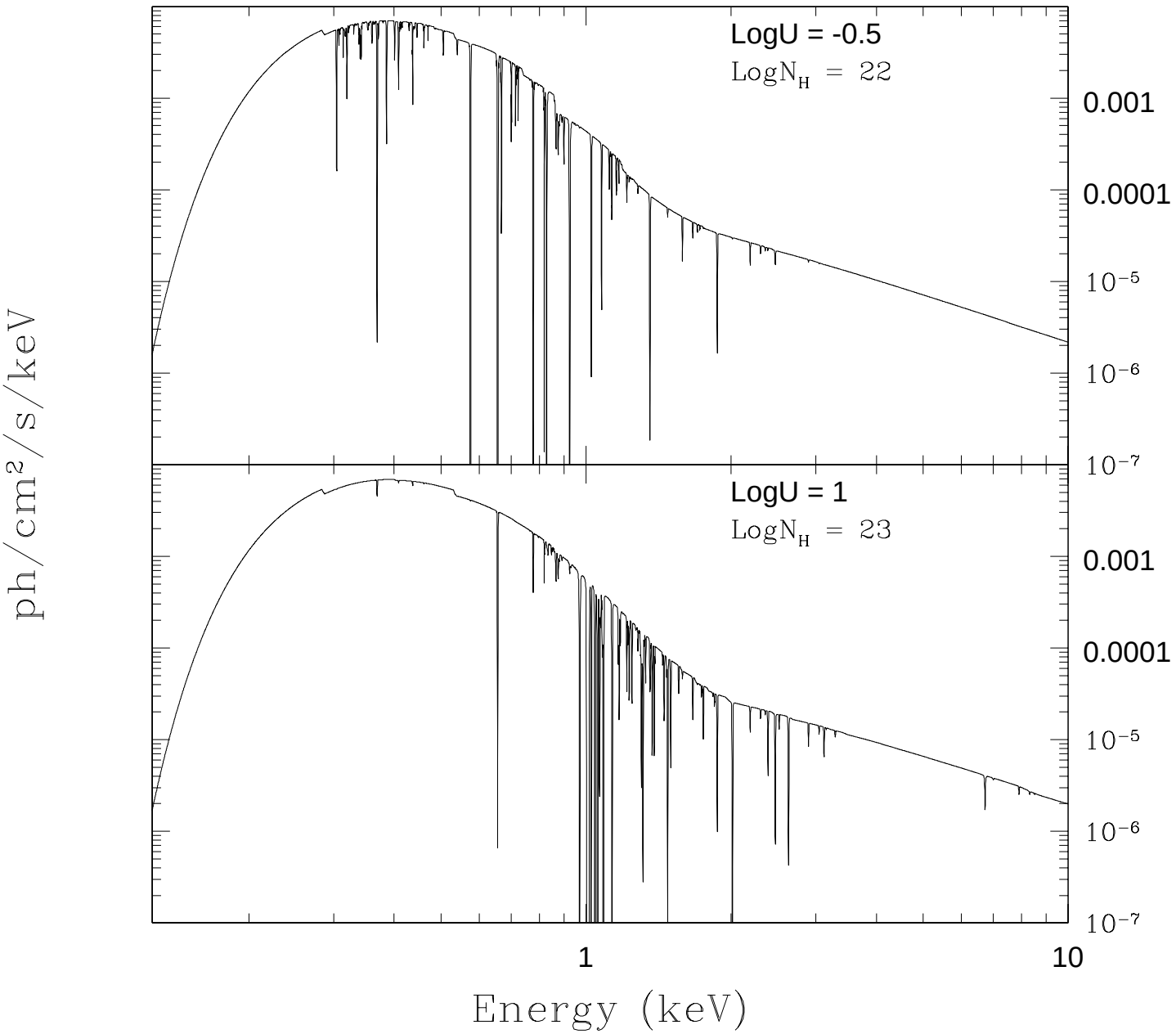
LogU = -0.5
LogN$_H$ = 22
LogU = 1
LogN$_H$ = 23
0.001
0.0001
10^{-5}
10^{-6}
10^{-7}
1
10
Energy (keV)
ph/cm^2/s/keV

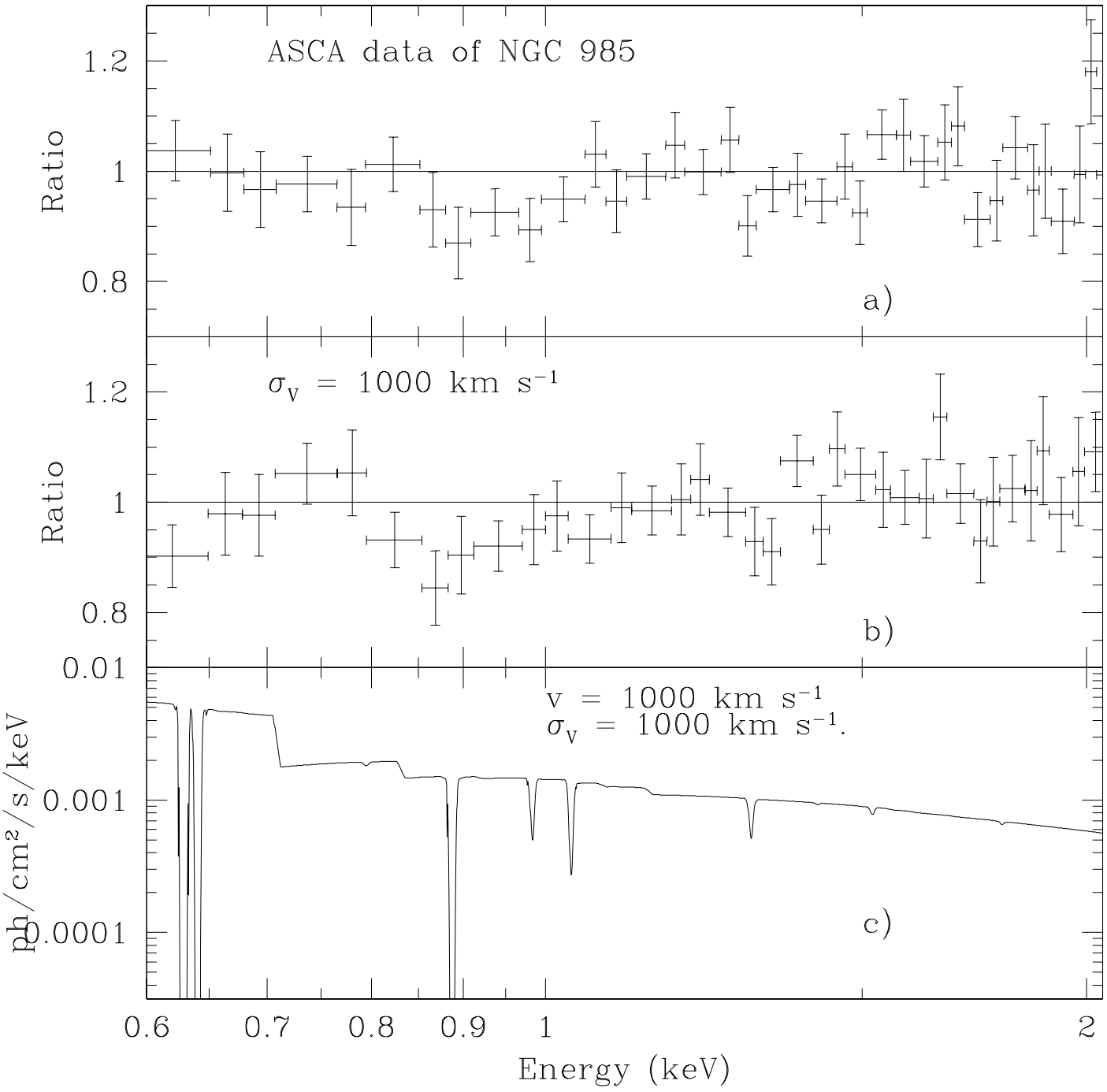
ASCA data of NGC 985
Ratio
1.2
1
0.8
a)
σ_v = 1000 km s^{-1}
Ratio
1.2
1
0.8
b)
0.01
v = 1000 km s^{-1}
σ_v = 1000 km s^{-1}.
ph/cm^2/s/keV
0.001
0.0001
c)
0.6
0.7
0.8
0.9
1
2
Energy (keV)

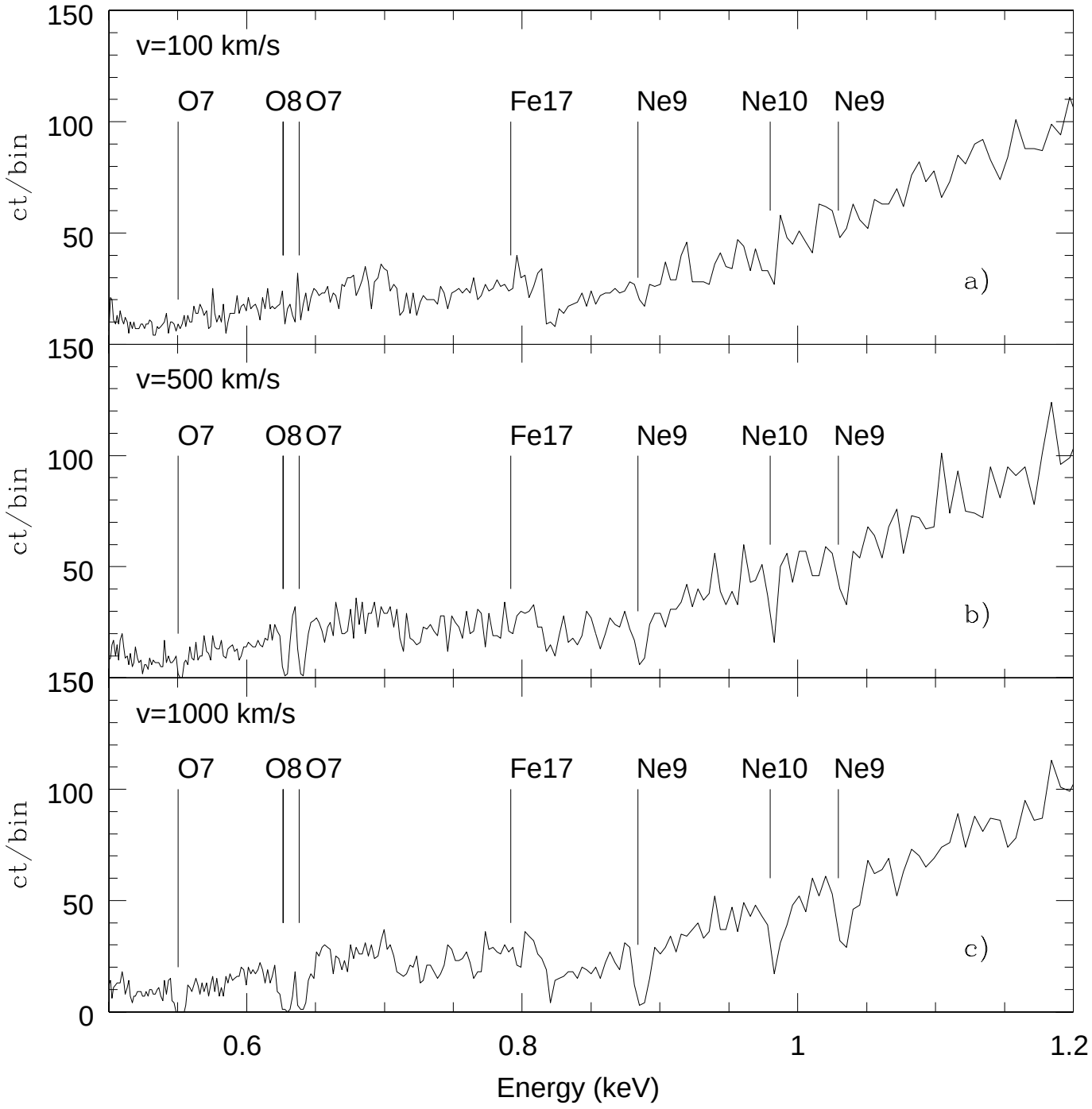
v=100 km/s
O7
O8
O7
Fe17
Ne9
Ne10
Ne9
a)
v=500 km/s
b)
v=1000 km/s
c)
ct/bin
150
100
50
0
0.6
0.8
1
1.2
Energy (keV)

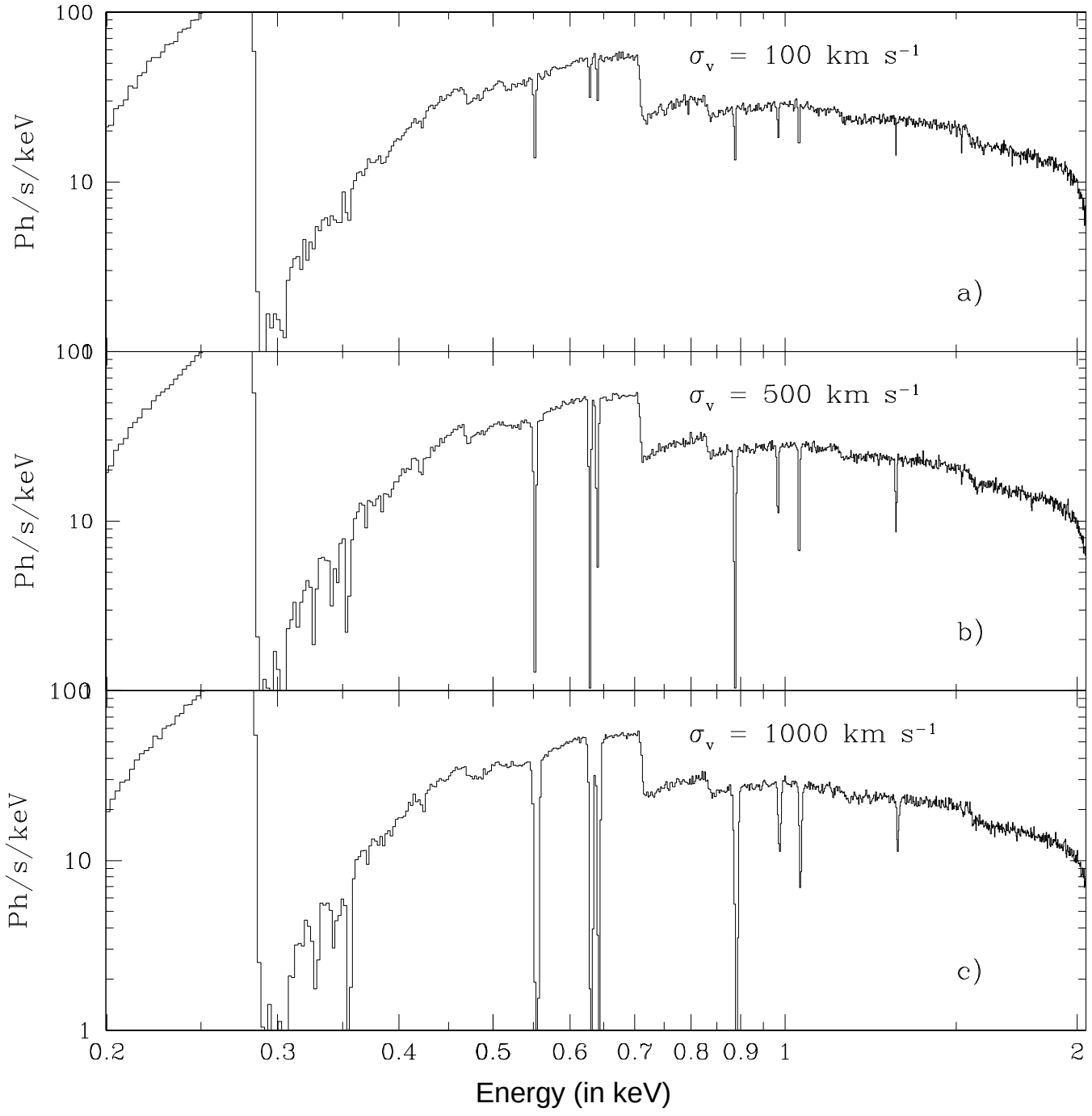
100
10
1
Ph/s/keV
σ_v = 100 km s^{-1}
a)
σ_v = 500 km s^{-1}
b)
σ_v = 1000 km s^{-1}
c)
0.2
0.3
0.4
0.5
0.6
0.7
0.8
0.9
1
2
Energy (in keV)

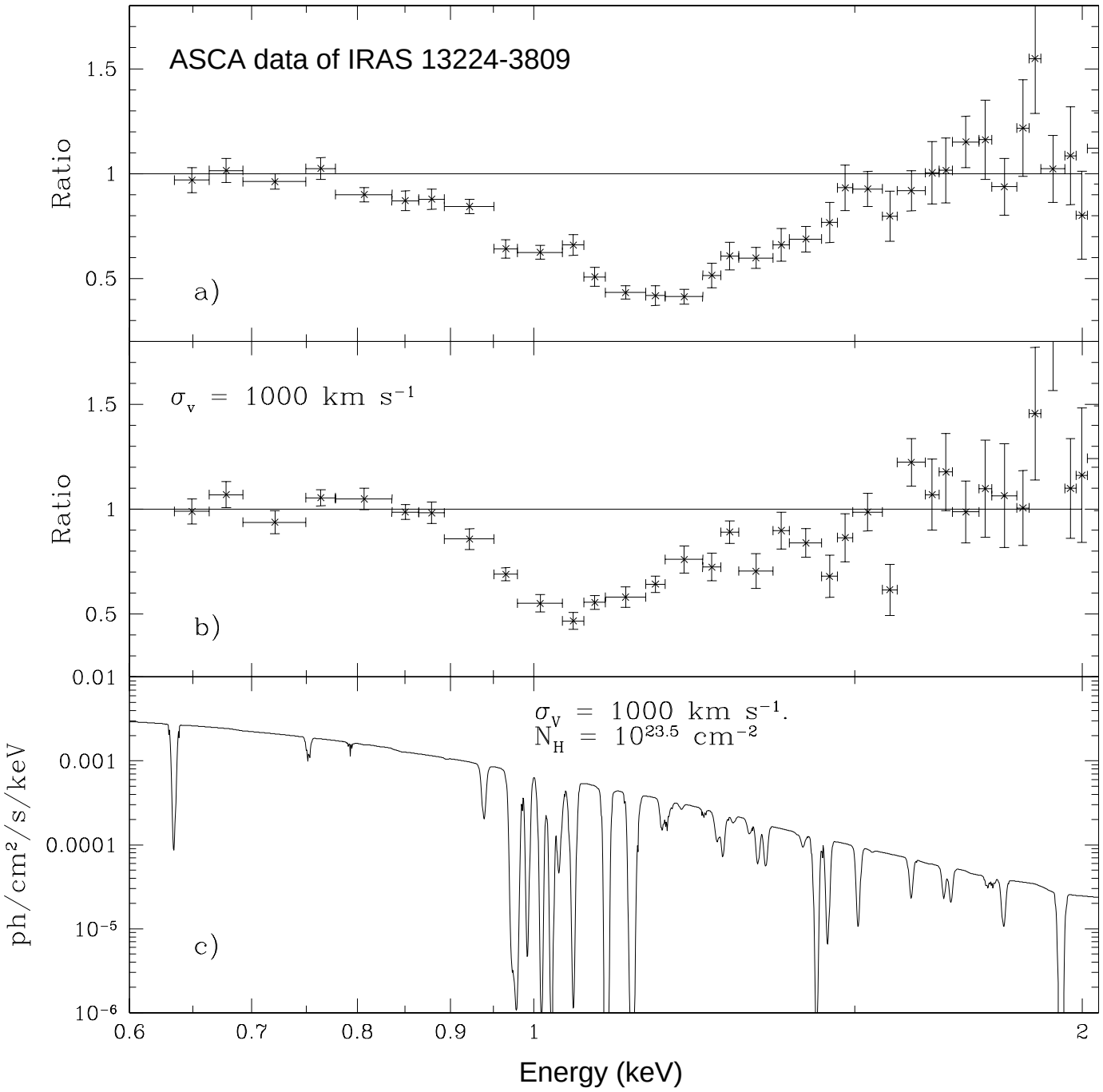
ASCA data of IRAS 13224-3809
Ratio
a)
σ_v = 1000 km s^{-1}
Ratio
b)
σ_V = 1000 km s^{-1}.
N_H = $10^{23.5}$ cm^{-2}
c)
ph/cm²/s/keV
Energy (keV)

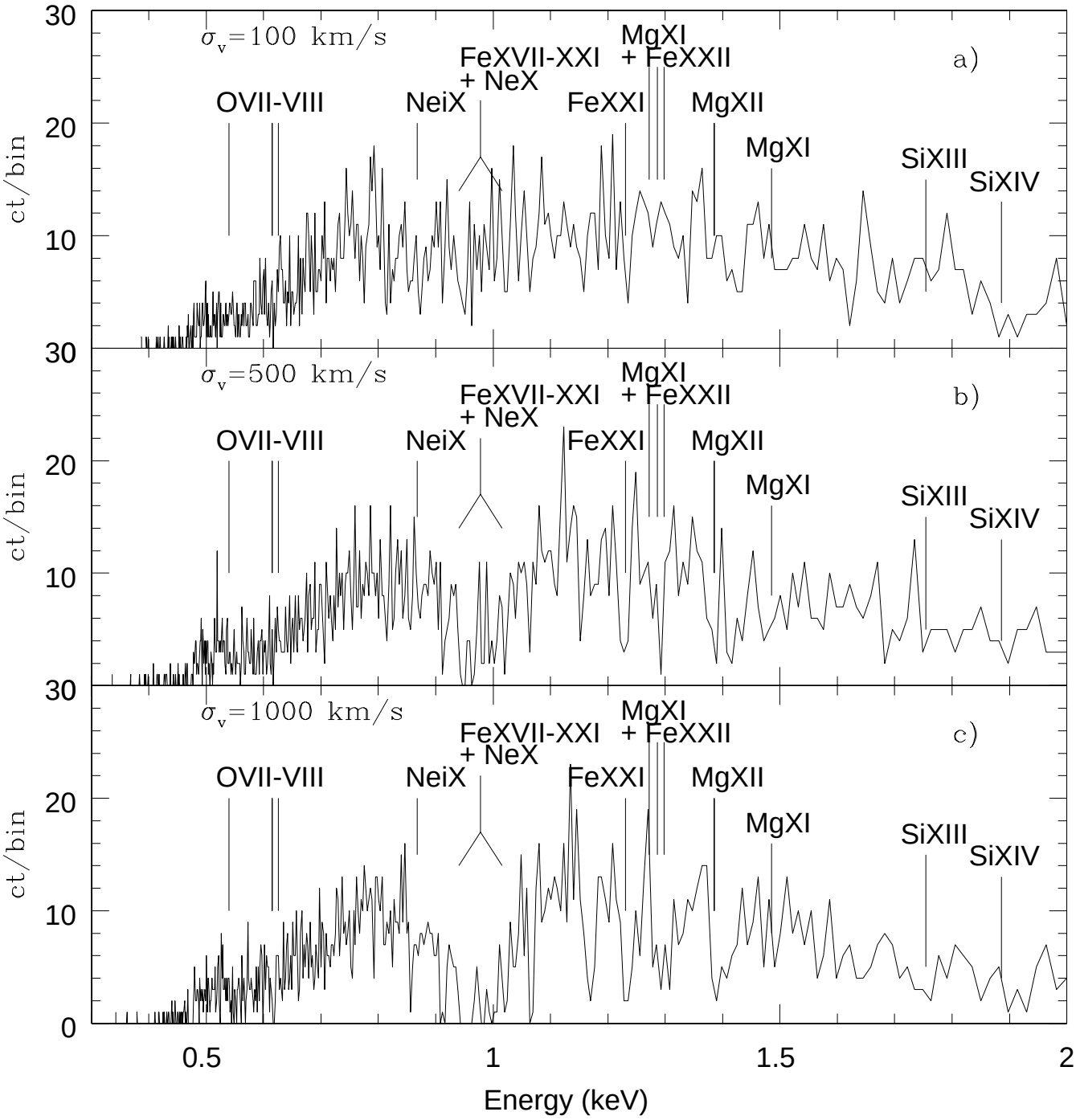
σ_v=100 km/s
a)
σ_v=500 km/s
b)
σ_v=1000 km/s
c)
OVII-VIII
NeiX
FeXVII-XXI
+ NeX
FeXXI
MgXI
+ FeXXII
MgXII
MgXI
SiXIII
SiXIV
ct/bin
Energy (keV)
0
10
20
30
0.5
1
1.5
2

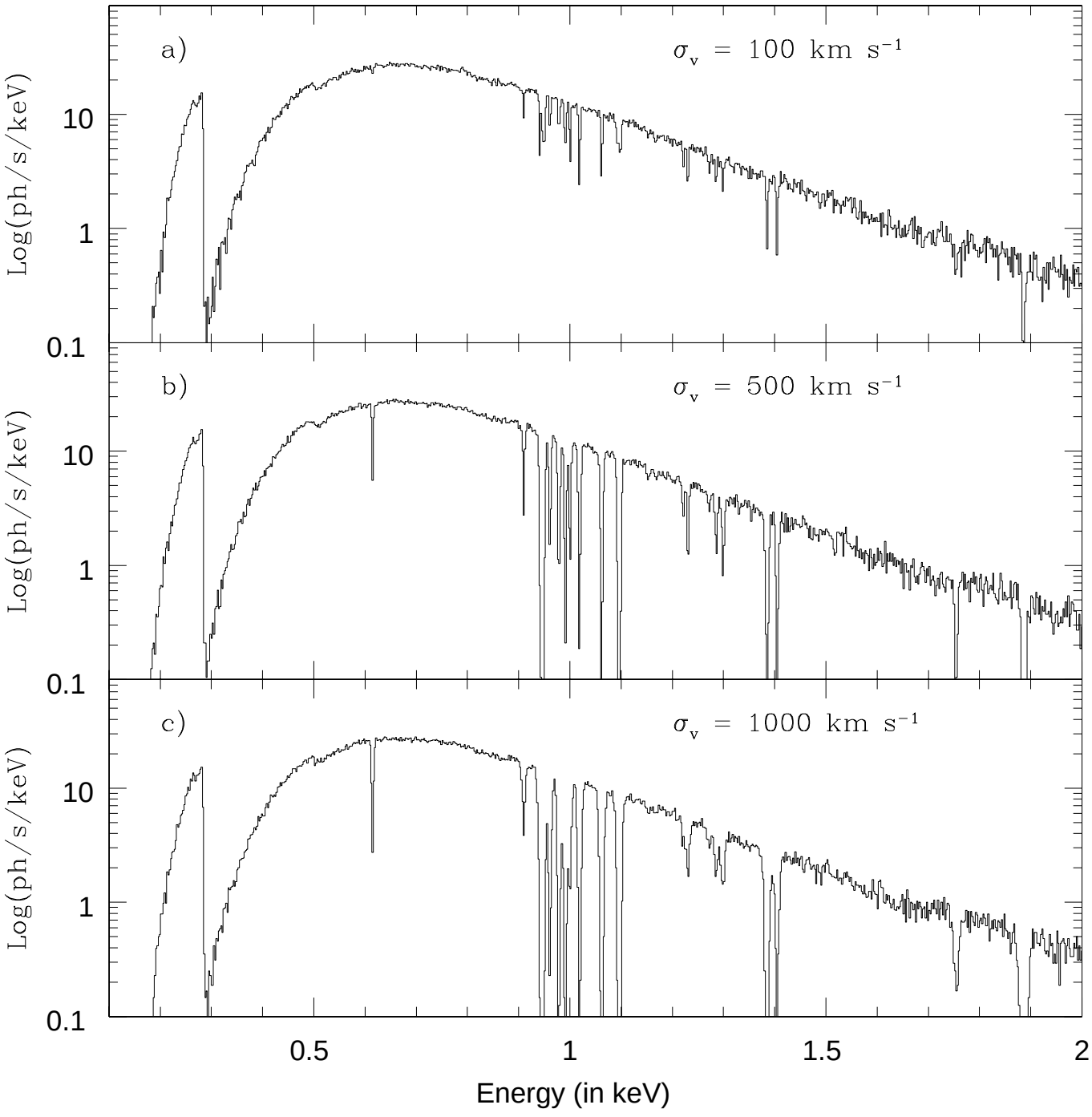
a)
σ_v = 100 km s^{-1}
b)
σ_v = 500 km s^{-1}
c)
σ_v = 1000 km s^{-1}
Log(ph/s/keV)
10
1
0.1
0.5
1
1.5
2
Energy (in keV)